

## SUPPLEMENTAL MATERIAL

### **Critical role of cytosolic DNA and its sensing adaptor STING in aortic degeneration, dissection, and rupture**

Wei Luo, MD<sup>1,2,#</sup>; Yidan Wang, MD, PhD<sup>1,2,#</sup>; Lin Zhang, MS<sup>1,2</sup>; Pingping Ren, MD, PhD<sup>1,2</sup>; Chen Zhang, MD<sup>1,2</sup>; Yanming Li, PhD<sup>1,2</sup>; Alon R. Azares, BS<sup>3</sup>; Michelle Zhang<sup>1</sup>; Jiao Guo, PhD<sup>1,2</sup>; Ketan B. Ghaghada, PhD<sup>4</sup>; Zbigniew A. Starosolski, PhD<sup>4</sup>; Kimal Rajapakshe, PhD<sup>5</sup>; Cristian Coarfa, PhD<sup>5,6</sup>; Yumei Li, PhD<sup>7</sup>; Rui Chen, PhD<sup>7,8,9</sup>; Keigi Fujiwara, PhD<sup>10</sup>; Jun-ichi Abe, MD, PhD<sup>10</sup>; Joseph S. Coselli, MD<sup>1,2,11</sup>; Dianna M. Milewicz, MD, PhD<sup>12</sup>; Scott A. LeMaire, MD<sup>1,2,11,\*</sup> and Ying H. Shen, MD, PhD<sup>1,2,11,\*</sup>

<sup>1</sup>Division of Cardiothoracic Surgery, Michael E. DeBakey Department of Surgery, Baylor College of Medicine, Houston, Texas, USA

<sup>2</sup>Department of Cardiovascular Surgery, Texas Heart Institute, Houston, Texas, USA

<sup>3</sup>Molecular Cardiology Research Lab, Texas Heart Institute, Houston, Texas, USA

<sup>4</sup>Department of Pediatric Radiology, Texas Children's Hospital, Houston, Texas, USA

<sup>5</sup>Department of Molecular and Cellular Biology, Baylor College of Medicine, Houston, Texas, USA

<sup>6</sup>Dan L. Duncan Cancer Center, Baylor College of Medicine, Houston, Texas, USA

<sup>7</sup>Human Genome Sequencing Center, Baylor College of Medicine, Houston, Texas, USA

<sup>8</sup>Department of Molecular and Human Genetics, Baylor College of Medicine, Houston, Texas, USA

<sup>9</sup>Department of Biochemistry and Molecular Biology, Baylor College of Medicine, Houston, Texas, USA

<sup>10</sup>Department of Biostatistics and Division of Internal Medicine, Department of Cardiology Research, The University of Texas MD Anderson Cancer Center, Houston, Texas, USA

<sup>11</sup>Cardiovascular Research Institute, Baylor College of Medicine, Houston, Texas, USA

<sup>12</sup>Division of Medical Genetics, Department of Internal Medicine, The University of Texas Health Science Center at Houston, Houston, Texas, USA

#These authors contributed equally.

### **Correspondence**

Ying H. Shen, MD, PhD, Department of Surgery, Baylor College of Medicine, One Baylor Plaza, BCM 390, Houston, Texas 77030. Phone: 832.355.9952; fax: 832.355.9951; email:

hyshen@bcm.edu; or: Scott A. LeMaire, MD, Department of Surgery, Baylor College of

Medicine, One Baylor Plaza, BCM 390, Houston, Texas 77030. Phone: 832.355.9942; fax:

832.355.9928; email: slemaire@bcm.edu.

## Supplemental Methods

### Human Tissue Study

Aortic tissue samples from patients with sporadic ATAAD and control aortic tissue samples were obtained from our existing aortic tissue bank. Patients with ATAAD caused by genetically triggered aortic disease, such as Marfan syndrome, or associated with bicuspid aortic valve were excluded from study enrollment. Characteristics of patients and control individuals are shown in Table 1. As previously described,<sup>1,2</sup> patient aortic tissues were collected during aortic repair surgery; aortic tissue is routinely excised from the anterior-lateral portion of the aortic wall (the outer wall of the false lumen in dissection cases) in the region of the aorta with the largest diameter, and a portion of this discarded tissue is collected for our aortic tissue bank. Control aortic tissue was collected from age-matched organ donors without aortic aneurysm, dissection, coarctation, or previous aortic repair (International Institute for the Advancement of Medicine, Jessup, PA). To minimize the effect of aortic damage caused by poor circulation, we selected donors with cardiac arrest for less than 60 minutes. The aortas were collected within 60 minutes of termination of life support, preserved in UW Belzer solution, and shipped to our lab on wet ice. The time from aorta collection to tissue processing and banking was less than 24 hours. The aortic tissue was processed as follows. Periaortic fat and intraluminal thrombus were trimmed from aortic tissue and rinsed with 0.9% normal saline. The aortic tissue was divided into several segments, which were then fixed in 10% formalin and embedded in paraffin for histologic analysis, embedded in optimal cutting temperature (OCT) compound for immunofluorescence staining, placed in RNAlater for RNA analysis, or snap-frozen in liquid nitrogen for protein extraction.

### Animal Studies

To generate a mouse model of sporadic AAD, we purchased male and female WT mice (C57BL/6J) and *Sting*-deficient mice (C57BL/6J-Tmem173gt/J, *Sting*<sup>gt/gt</sup>) from The Jackson

Laboratory (Bar Harbor, ME). Sporadic AAD was induced by challenging mice with a combination of a HFD and AngII, as described previously.<sup>1,2</sup> Four-week-old male and female WT mice (n = 50) and *Sting*<sup>gt/gt</sup> mice (n = 39) were challenged with a HFD (20% protein, 40% carbohydrate, 40% fat, and 1.25% cholesterol; Research Diets, Inc., D12108C, New Brunswick, NJ) for 8 weeks and 2,000 ng/min/kg AngII (cat# A2900-50MG, Sigma-Aldrich Corp., St. Louis, MO) infusion during the last 4 weeks through an osmotic minipump (Model 2004; ALZA Scientific Products, Mountain View, CA). Mice fed a chow diet for 8 weeks and infused with saline during the last 4 weeks were used as unchallenged controls.

For experiments with amlexanox, WT mice were challenged as described above and were given either amlexanox (100 mg/kg dissolved in sunflower oil) or sunflower oil (control) daily by oral gavage during the AngII infusion period. At the end of the challenge period, mice were euthanized, and their aortas were exposed, cleaned, extracted, and imaged for diameter measurement and disease evaluation. The aortic segments were embedded in OCT compound for histology and immunofluorescence staining or were snap-frozen for protein analysis.

We determined the sample size of mice based on preliminary data that indicated the overall incidence of AAD in all aortic segments was 82% for challenged WT mice, 28% for challenged *Sting*<sup>gt/gt</sup> mice, and 45% for challenged WT mice that received amlexanox. To show that the difference in the incidence of AAD between these groups was statistically significant (at  $\alpha = 0.05$  with 80% power), we included 18 to 20 mice in each challenged group.

To generate a mouse model of CaCl<sub>2</sub>-induced abdominal aortic aneurysm (AAA), we purchased 12-week-old male C57BL/6 mice and *Sting*-deficient mice (C57BL/6J-Tmem173gt/J, *Sting*<sup>gt/gt</sup>) from The Jackson Laboratory (Bar Harbor, ME). AAA was induced by the periaortic application of 0.5 M CaCl<sub>2</sub>, as previously described.<sup>3</sup> Briefly, the infrarenal aorta was isolated, and a small piece of gauze soaked in 0.5 M CaCl<sub>2</sub> was applied perivascularly for 15 minutes. Mice in the sham group received one treatment of 0.5 M NaCl-soaked gauze for 15 minutes.

After the application of soaked gauze, 0.9% sterile saline was used to wash the surrounding tissue, and the incision was sutured.

### **In Vivo Computed Tomography (CT) Imaging**

High-resolution contrast-enhanced CT imaging was performed in a subset of mice for the *in vivo* visualization of aortic pathology. Imaging was performed on a small animal micro-CT scanner (Inveon, Siemens Inc., Knoxville, TN). Mice were anesthetized with 3% to 4% isoflurane, positioned prone on the CT cradle, and scanned while free breathing under anesthesia by using 1% to 1.5% isoflurane delivered via a face-cone. Respiratory rate was monitored by using a pneumatic pressure pad placed underneath the animal. Mice were intravenously administered a long circulating blood-pool liposomal-iodine (liposomal-I, 1.1 g I/kg) contrast agent for CT angiography.<sup>4,5</sup> The long blood half-life of the contrast agent (approximately 48 hours) allows uniform opacification of the blood circulatory system for a prolonged period, thereby enabling high-resolution vascular imaging.<sup>6</sup> Images were acquired by using the following scan parameters: 50 kVp, 0.5 mA, 400 ms X-ray exposure, 540 projections, 70  $\mu\text{m}$  isotropic spatial resolution, and 10 minutes scan time. CT images were analyzed in Osirix (version 5.8.5 64-bit; Pixmeo, Bernex, Switzerland). Three-dimensional curved multiplanar reformation images were generated to visualize the entire length of the aorta for the presence of dilation, aneurysm, or dissection. The aorta was segmented on CT images in ITK-SNAP (version 3.4.0) and post-processed for mesh smoothing in Meshmixer (version 10.9.332) for three-dimensional visualization.

### **Aortic Diameter Measurement**

In euthanized mice, the aorta was exposed and rinsed with cold phosphate-buffered saline (PBS), and the periaortic tissue was removed as described previously.<sup>1,2</sup> Then, the aorta was excised and further cleaned and rinsed with cold PBS to remove any residual blood in the

lumen. In the mouse model of sporadic AAD, we evaluated the ascending, arch, descending thoracic, suprarenal abdominal, and infrarenal segments of the excised aorta. Images of the aorta were obtained by using an Olympus SZX7 microscope at a magnification of 0.4X (scale bar = 2 mm), and the diameter of each aortic segment was measured with the use of DP2-BSW software (Olympus Life Science Solutions, Center Valley, PA) by two independent observers who were blinded to the animal groups. The mean diameter of the different regions was calculated and compared among the groups. In the mouse model of CaCl<sub>2</sub>-induced AAA, we measured the external diameter of the largest portion of the infrarenal aorta.

### **Definition of Aortic Dilatation, Aortic Aneurysm, and Aortic Dissection**

For each aortic segment of WT or *Sting<sup>gt/gt</sup>* mice, dilatation was defined as an aortic diameter  $\geq 1.25$  but  $< 1.5$  times the mean aortic diameter of the segment in unchallenged mice with the same genetic background. Aneurysm was defined as an aortic diameter  $\geq 1.5$  times the mean aortic diameter of the segment in unchallenged mice with the same genetic background. Aortic dissection was defined as the presence of hematoma within the aortic wall detected on gross examination or as the presence of layer separation within the aortic media or medial-adventitial boundary (with a false lumen hematoma) detected upon histologic examination of the aorta. Aortic rupture and premature death were documented.

### **Classification of AAD Severity**

The severity of AAD was classified by using our previously reported<sup>2</sup> modification of the classification system described by Daugherty and colleagues<sup>7</sup>: normal aorta, dilated aorta, aortic aneurysm without dissection, aortic dissection (as indicated by intramural thrombus) without aneurysm, aortic aneurysm with dissection, or ruptured aorta. We defined AAD as the presence of aneurysm, dissection, or rupture. Severe AAD was defined as the presence of dissection or rupture. Aneurysmal tissue was evaluated by 4 independent observers who were blinded to the

experimental groups. In the case of a discrepancy, the observers discussed the case and agreed on the classification.

### **Aortic Contractility**

We examined aortic contractility in aortas from challenged or unchallenged WT and *Sting<sup>gt/gt</sup>* mice. In euthanized mice, the aorta was exposed, perfused with ice-cold PBS, and transferred to a physiologic salt solution (PSS) containing (in g/L) NaCl 6.954, KCl 0.35, MgSO<sub>4</sub>·7H<sub>2</sub>O 0.289, NaHCO<sub>3</sub> 2.1, KH<sub>2</sub>PO<sub>4</sub> 0.161, EDTA 0.010, glucose 1.091, and CaCl<sub>2</sub>·7H<sub>2</sub>O 0.368. The aorta was cleaned without damaging the endothelium. The ascending aorta was excised and cut into 2-mm segments by using a ruler under the microscope as a guide. The harvested ascending aortic segment was mounted onto metal stirrups of a wire myograph machine (DMT, Ann Arbor, MI) and incubated at 37°C for 60 minutes in equilibrated carbogen buffer (95% O<sub>2</sub>, 5% CO<sub>2</sub>) that was refreshed every 20 minutes. The aortic segment was then stimulated with phenylephrine in high potassium PSS solution containing (in g/L) KCl 9.223, MgSO<sub>4</sub>·7H<sub>2</sub>O 0.289, NaHCO<sub>3</sub> 2.1, KH<sub>2</sub>PO<sub>4</sub> 0.161, EDTA 0.010, glucose 1.091, and CaCl<sub>2</sub>·7H<sub>2</sub>O 0.368. The segment was then washed with PSS. The process was repeated 4 times with an increasing dose of phenylephrine (10<sup>-9</sup> M to 10<sup>-5</sup> M). A cumulative concentration-response curve to phenylephrine was constructed with LabChart to evaluate the contractile function of the ascending aorta.

### **Hematoxylin and Eosin Staining and Elastic Fiber Staining**

Aortic sections were stained with hematoxylin and eosin (Sigma-Aldrich) and Verhoeff–Van Gieson (Sigma-Aldrich) according to the manufacturer's instructions. The aortic sections were examined by 2 independent observers who were blinded to the experimental groups. The extent of elastic fiber fragmentation was scored on a scale of 0 to 3 (0 = none, 1 = minimal, 2 = moderate, and 3 = severe).

### **ROS Detection**

As previously described,<sup>8</sup> aortic tissue sections were stained with dihydroethidium (DHE; 10  $\mu$ M, Thermo Fisher) at 37°C for 30 minutes in the dark. The presence of ROS was detected by using a fluorescence microscope (Olympus).

### **Immunofluorescence Staining and Imaging**

OCT-embedded aortic sections or treated cells on slides were fixed with Cytfix (BD Biosciences, San Jose, CA) and permeabilized with Perm/Wash (BD Biosciences). Nonspecific staining was reduced by blocking with 10% donkey serum. The sections or cells were then incubated with primary antibody at room temperature for 2 hours or at 4°C overnight, washed with PBS, and incubated with secondary antibody. Antibodies used for immunostaining are listed in Supplemental Table 2. Nuclei were counterstained with 4',6-diamidino-2-phenylindole (DAPI). The slides were mounted with Dako Fluorescence Mounting Medium (Dako North America, Inc., Carpinteria, CA). Slides of sections or treated cells incubated with secondary antibody alone were used as negative controls. Tissue sections were examined by using a Leica microscope (Leica Microsystems Inc., Buffalo Grove, IL) or a Leica SP5 confocal microscope (Leica).

### **TUNEL Assay and Immunofluorescence Staining**

To study apoptosis using an in situ cell death detection kit (Roche Applied Science, Indianapolis, IN), we performed TUNEL staining according to the manufacturer's instructions. In addition, we performed TUNEL staining with immunofluorescence co-staining. First, frozen sections of aorta or cells were fixed with Cytfix (BD Biosciences), permeabilized with Perm/Wash (BD Biosciences), and subjected to TUNEL staining. After TUNEL staining, sections or cells were blocked with 10% donkey serum at room temperature for 1 hour and stained with

anti-SM22- $\alpha$  antibody at 4 °C overnight. Sections or cells were then stained with secondary antibody at room temperature for 1 hour. Tissue sections or cells were observed by using a Leica SP5 confocal microscope (Leica). For each aorta or cell treatment condition, images were captured from 3 randomly selected views. For each image, the number of positive cells and the number of total cell nuclei were quantified, and the percentage of positive cells was calculated.

### **Transmission Electron Microscopy**

Select samples of aortic tissue were placed in fixation solution (2.5% paraformaldehyde, 2.5% glutaraldehyde, 2 mM CaCl<sub>2</sub> in 0.1 M cacodylate buffer, pH 7.4) for 1 to 2 days. Samples were rinsed in 0.1 M sodium cacodylate buffer and post-fixed in 1% OsO<sub>4</sub> for 1 hour. Samples were then dehydrated in ethanol and embedded in epoxy resin. Sections were cut at nominal thickness (60 nm) and observed under a transmission electron microscope (H-7500, Hitachi, Brisbane, CA).

### **MMP Activity Determined by Using In Situ Zymography and Gel Zymography**

MMP activity in the aortic wall was determined by using gelatin conjugated with quenched fluorescein (DQ gelatin; Invitrogen Corporation, Carlsbad, CA) as a substrate. Briefly, frozen aortic sections were overlaid with 0.1 mg/mL DQ gelatin that was dissolved in 1% low-melting multi-purpose agarose (Roche, Grenzach, Germany) containing reaction buffer and DAPI. The slides were kept in a moist chamber at 37°C for 2 hours. Fluorescence microscopy was used to examine green fluorescence indicative of gelatinase activity.

MMP activity in cell lysates was analyzed by using gel zymography. Protein samples (10  $\mu$ l each) were mixed in Novex Tris-Glycine Sodium Dodecyl Sulfate (SDS) Sample Buffer (Thermo Fisher) and then loaded onto Novex 10% Zymogram Plus (Gelatin) protein gels for separation. Gels were electrophoresed at 125 volts for 2 hours. After electrophoresis, the gels were renatured in Zymogram renaturing buffer (Thermo Fisher) at room temperature for 30

minutes and incubated overnight at 37°C in Zymogram developing buffer (Thermo Fisher). The gels were stained with Coomassie Blue staining solution (0.1% Coomassie R250 in 40% ethanol, 10% acetic acid) for 2 hours and then destained twice for 30 minutes in destaining solution (10% ethanol and 7.5% acetic acid). The presence of a clear band on a dark background indicated MMP activity. We used a CanoScan 9950F flatbed scanner to obtain images of the stained gels.

### **Western Blot Analysis**

Protein lysates from treated cells or aortic tissues were prepared as previously described.<sup>1,2</sup> Protein samples (15 µg per lane) were subjected to SDS polyacrylamide gel electrophoresis and were transferred to polyvinyl difluoride membranes. The membranes were blocked for 1 hour in blocking solution comprising Tris-buffered saline containing 5% nonfat dried milk and 0.5% Tween 20 and then were incubated with a primary antibody. Next, the membranes were washed and incubated with horseradish peroxidase–conjugated anti-rabbit or anti-mouse secondary antibody. Antibodies used for western blotting are listed in Supplemental Table 2. Protein bands were visualized by using Clarity Enhanced Chemiluminescence (Bio-Rad Laboratories, Inc., Hercules, CA) and were exposed with HyBlot ES autoradiography film (Denville Scientific Inc., Holliston, MA). The blots were quantified with densitometry by using the Quantity One imaging program (Bio-Rad). Protein levels were normalized to those of β-actin and were expressed as a percentage of the untreated control.

### **Bulk RNA-Seq and Bioinformatics Analysis**

RNA was extracted from aortas of WT mice and *Sting*<sup>gt/gt</sup> mice by using the RNeasy tissue kit according to the manufacturer's instructions (74104, Qiagen). An RNA-seq library was made with the KAPA Stranded mRNA-Seq kit (KK8420, KAPA biosystems). Briefly, poly-A RNA was

purified from total RNA by using oligo-dT beads, converted to 1<sup>st</sup>-strand cDNA and then 2<sup>nd</sup> cDNA (labeled with dUTP), made into a cDNA library, amplified, and sequenced on Novaseq. The strand labeled with dUTP was not amplified, allowing for strand-specific sequencing. FASTQ sequence data were mapped to mouse genome mm10. The reads per gene were counted by using “HTseq” (<https://htseq.readthedocs.io>, version 0.6.0). Gene expression, presented as fragments per kilobase of transcript per million mapped reads (FPKM), was estimated by using “Cufflinks” (<http://cole-trapnell-lab.github.io/cufflinks>).<sup>9</sup> Principal components analysis was performed by using the “Prcomp” function of R. Differentially expressed genes (DEGs) were identified by using R package “EdgeR”<sup>10</sup> with a threshold of fold change >2 and FDR<0.05. Differential expression was assessed for each gene by using an exact test analogous to the Fisher exact test. FDR was adjusted by using the Benjamini-Hochberg correction. Gene ontology (GO) analysis was performed by using an R package “ClusterProfiler.”<sup>11</sup>

### **Single-cell RNA-Seq and Bioinformatics Analysis**

The excised mouse aortas were digested in enzyme cocktail (including collagenase type II [LS004176, Worthington], collagenase type XI [C7657, Sigma-Aldrich], hyaluronidase [H3506, Sigma-Aldrich], and elastase [LS002290, Worthington]) for 1.5 hours at 37°C to make a single-cell suspension. The cells were sorted with flow cytometry to select viable single cells and achieve ≥95% viability. The single-cell suspensions from 3 mice per group were pooled together as one sample (5000-10000 cells/sample) and *dispensed* onto the Chromium Controller (10x Genomics). The single-cell RNA-seq library was constructed by using the Chromium Single Cell 3' v2 Reagent Kit (10x Genomics). Cells were mixed with barcoded primer-linked gel beads. Each cell was uniquely barcoded with an index, and every transcript within one cell was uniquely barcoded with a unique molecular identifier (UMI). The cDNAs were pooled, truncated, and amplified to generate cDNA libraries that were sequenced by using a Next Generation

sequencer NovaSeq 6000 (Illumina) in a pair-end fashion to reach more than 80,000 reads per cell.

FASTQ sequence data were processed to obtain a UMI count in each cell by using “Cell Ranger.” A mouse reference genome (mm10) was used for gene alignment. Subsequent single-cell RNA-seq analysis was performed in R package “Seurat” (version 3.0.0).<sup>12</sup> Cells with low quality (<200 or >5000 genes per cell and >25% mitochondrial genes in the cell) were filtered out. Data were normalized and scaled within each sample, and canonical correlation analysis was performed to integrate data across samples. Cell population deconvolution was performed by the dimensional reduction and shared nearest neighbor (SNN) modularity clustering algorithm. We defined the cell clusters based on a set of highly expressed differential/conservative/cell marker genes. SMC clusters were defined according to the high expression levels of SMC marker genes (*Acta2*, *Myh11*, *Mylk*). Macrophage clusters were defined according to the high level of macrophage marker genes (*Cd68*, *Adger1*, *F13a1*) but not SMC genes. DEGs in each cluster across different conditions were identified by using the “FindMarkers” function in Seurat. Within each cluster, DEGs between two groups of cells were identified by using a Wilcoxon rank sum test. Adjusted p-values were calculated on the basis of the Bonferroni correction by using all features in the dataset. Genes with a  $p\_val\_adj < 0.05$  were considered as DEGs. GO analysis was performed by using an R package “ClusterProfiler.”<sup>11</sup>

### **Cell Culture and Transfection**

Human thoracic aortic SMCs (ATCC, Manassas, VA) were cultured in smooth muscle cell medium (Cell Applications, Inc. San Diego, CA) with 10% fetal bovine serum (ThermoFisher). SMCs were pretreated with or without 20  $\mu$ M zVAD (Santa Cruz) and were then treated with hydrogen peroxide ( $H_2O_2$ ) or transfected with SMC DNA by using Lipofectamine 2000 (Thermo Fisher) at the given concentrations for 24 hours. SMCs were transfected with siRNA or plasmid

DNA by using Lipofectamine 2000 (Thermo Fisher) according to the manufacturer's instructions. STING siRNA, TBK1 siRNA, and IRF3 siRNA were purchased from Thermo Fisher, and STING and TBK1 plasmids were purchased from GenScript and Addgene. SMCs were pretreated for 1 hour with amlexanox at the given concentrations, followed by treatment with 500  $\mu\text{M}$   $\text{H}_2\text{O}_2$  or transfection with 2  $\mu\text{g}/\text{mL}$  SMC DNA.

Human acute monocytic leukemia cells (THP-1) were cultured in RPMI 1640 (Thermo Fisher) supplemented with 10% heat-inactivated fetal bovine serum. To stimulate the differentiation of THP-1 cells into adherent macrophages, we treated cells with 100 nM phorbol 12-myristate 13-acetate (PMA, Sigma-Aldrich) in RPMI for 24 hours. The cells were then cultured in fresh RPMI complete for an additional 48 hours. Macrophages were transfected with 100 nM STING siRNA, IRF3 siRNA (Invitrogen), or scrambled siRNA by using Lipofectamine RNAiMax (Life Technologies) according to the manufacturer's instructions. After a 24-hour transfection period, the transfected cells were transfected a second time with SMC DNA by using Lipofectamine 2000 (Thermo Fisher). Transfection efficiency was confirmed with western blot analysis. Macrophages were pretreated for 1 hour with amlexanox (50  $\mu\text{M}$ ) and were then transfected with 2  $\mu\text{g}/\text{mL}$  SMC DNA.

### **Aortic SMC DNA Isolation and Transfection**

To induce DNA damage, we treated aortic SMCs with  $\text{H}_2\text{O}_2$  for 24 hours. DNA from SMCs treated with 500  $\mu\text{M}$   $\text{H}_2\text{O}_2$  was isolated by using a commercial DNA isolation kit (Invitrogen) according to the manufacturer's instructions. Then, we transfected SMCs and THP-1 derived macrophages with varying amounts of the DNA isolated from SMCs by using Lipofectamine 2000 (Life Technology) as a carrier. As described in previous studies,<sup>13</sup> we harvested the supernatant and lysed the cells 4 hours later.

### **Macrophage Phagocytosis of Aortic SMCs**

Aortic SMCs were first labeled with Edu (5-ethynyl-2'-deoxyuridine) for 24 hours. These Edu-labeled SMCs were then added into the insert of a 24-well transwell (0.4  $\mu\text{m}$ , *Corning, Falcon, catalog number 3470*) and treated with 500  $\mu\text{M}$   $\text{H}_2\text{O}_2$  for 24 hours to induce cell injury. THP-1-derived macrophages were pre-plated onto the 24-well plate. The macrophages and SMCs were co-cultured without direct cell contact. Untreated SMCs were used as controls.

### **In Vitro DNase I Treatment**

In a separate set of experiments with the co-culture system described above, SMCs in the upper insert were treated with DNase I (1  $\mu\text{g}/\text{mL}$ ) while simultaneously being treated with 500  $\mu\text{M}$   $\text{H}_2\text{O}_2$ .

### **Annexin V/Propidium Iodide Staining**

Cell death was detected by performing flow cytometry analysis of cells stained with annexin V (apoptotic cell marker) and propidium iodide (PI) (necrotic cell marker). Staining was accomplished with the use of an annexin V-FITC/PI staining kit (11858777001, Roche). Treated cells were harvested, washed with PBS, and stained with annexin V-FITC and PI in the dark at room temperature for 15 minutes. The samples were examined immediately on a flow cytometer (BD Biosciences), and the data were analyzed by using BD FACSDiva and Tree Star FlowJo software.

### **Real-time Quantitative RT-polymerase Chain Reaction (PCR)**

Total RNA from the aortic SMC DNA-treated macrophages was extracted with a commercial kit (Invitrogen) according to the manufacturer's instructions. The mRNA was reverse-transcribed into cDNA by using the iScript cDNA synthesis kit (Bio-Rad). Real-time PCR was performed by using the Real-Time PCR System (Bio-Rad). The primers for human *MMP9* were 5-TGT ACC

GCT ATG GTT ACA CTC G-3 (forward) and 5-GGC AGG GAC AGT TGC TTC T-3 (reverse); the primers for *18S rRNA* were 5- GTA ACC CGT TGA ACC CCA TT -3 (forward) and 5- CCA TCC AAT CGG TAG TAG CG -3 (reverse). The mRNA levels were acquired from the value of the threshold cycle (Ct) of *MMP9* and were normalized against the Ct of GAPDH.

### **Chromatin Immunoprecipitation Assay**

The chromatin immunoprecipitation assay was performed as previously described<sup>14,15</sup> by using the EZ-ChIP Kit according to the manufacturer's protocol (EMD Millipore Corp., Billerica, MA). In brief, aortic SMC DNA-treated macrophages were incubated with 1% formaldehyde at room temperature for 10 minutes to cross-link the DNA-protein complexes. Glycine was added to each sample to quench the unreacted formaldehyde. The cells were washed, harvested, and lysed. Cell lysates were sonicated and centrifuged to produce chromatin fragments that were 200 to 1000 base pairs long.<sup>14</sup> Immunoprecipitation was performed with an anti-IRF3 antibody-protein A-agarose slurry (IgG was used as the negative control). The immunocomplex beads were washed sequentially with low-salt wash buffer, high-salt wash buffer, LiCl wash buffer, and Tris-EDTA buffer. The immunocomplex was eluted with elution buffer (100 mmol/L NaHCO<sub>3</sub>, 1% SDS). The eluted immunocomplex and the input were incubated with 200 mM NaCl at 65°C overnight to reverse the cross-linking and then were incubated with proteinase K to digest the remaining proteins. The DNA was recovered by performing phenol/chloroform/isoamyl alcohol extraction and was used as a template for PCR.<sup>16</sup> To quantify the DNA, we performed real-time quantitative PCR and analyzed the results by using the comparative delta Ct method. Gel electrophoresis in 1.5% agarose gel was used to examine the size and purity of the PCR products. The primers used for the IRF3 binding site in the 5'-flanking region of the human *MMP9* gene were 5'- CAGTGG AATTCCCCAGCCTT -3' (forward) and 5'- TAATGATCCCCCTGGCCCAT-3' (reverse).

### **Measurement of Cytosolic dsDNA Concentration in Cultured SMCs or Aortic Tissue**

To avoid the contamination of mitochondrial DNA released into the cytosol, cytosolic DNA was isolated from aortic tissue or cultured SMCs by using a Mitochondria Isolation Kit (89801, Thermo Fisher), which protects mitochondria from damage. Briefly, a single-cell suspension from aortic tissue or cultured SMCs was centrifuged at 800 x g for 3 minutes at 4°C, and the supernatant was then discarded. Mitochondria Isolation Reagent A was added, and the tube was vortexed at medium speed for 5 seconds and incubated on ice for exactly 2 minutes. Mitochondria Isolation Reagent B was added, and the tube was vortexed at maximum speed for 5 seconds. The tube was incubated on ice for 5 minutes and vortexed at maximum speed every minute. Mitochondria Isolation Reagent C was added, and the tube was inverted several times to mix. The tube was centrifuged at 1000 x g for 10 minutes at 4°C. The pellet, which contained nuclei and cell debris, was discarded. The supernatant that contained cytosolic DNA and mitochondria was transferred to a new tube and then centrifuged at 12,000 x g for 15 minutes at 4°C. The supernatant, which contained cytosolic DNA, was transferred to a new tube, and the pellet that contained mitochondria was discarded. We then used the Monarch® PCR & DNA Cleanup Kit (New England Biolabs, T1030S) to remove any remaining mitochondria or lysosome contamination. The concentration of cytosolic dsDNA was measured by using a PicoGreen Assay Kit (P7589, Thermo Fisher) according to the manufacturer's instructions.

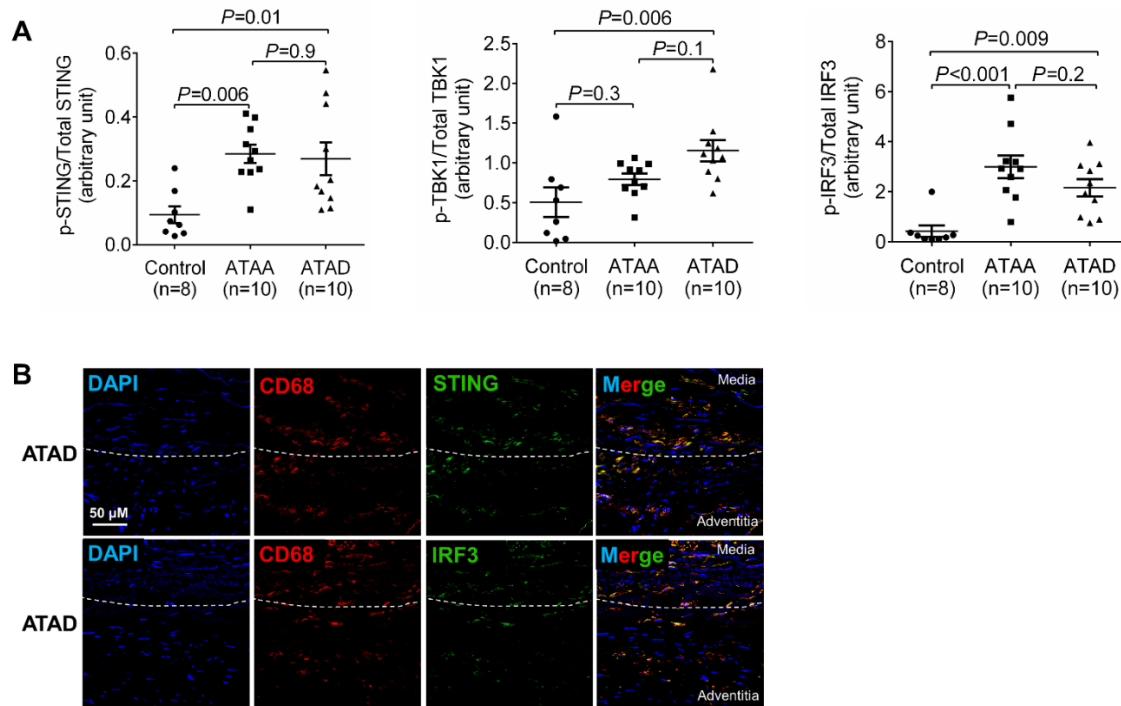
### **Immunofluorescence Staining to Detect Cytosolic DNA**

To detect cytosolic DNA in cultured SMCs, we triple-stained treated SMCs for DNA, mitochondrial marker, and lysosomal marker.<sup>16</sup> SMCs were first incubated with MitoTracker (Thermo Fisher) at 37°C for 30 minutes. SMCs were then fixed and permeabilized with BD Cytofix/Cytoperm solution (BD Biosciences) and blocked in 10% donkey serum. Next, SMCs were incubated with anti-LAMP1 antibody and anti-dsDNA antibody, followed by incubation with a fluorescently labeled secondary antibody. Although the anti-dsDNA antibody can also bind to

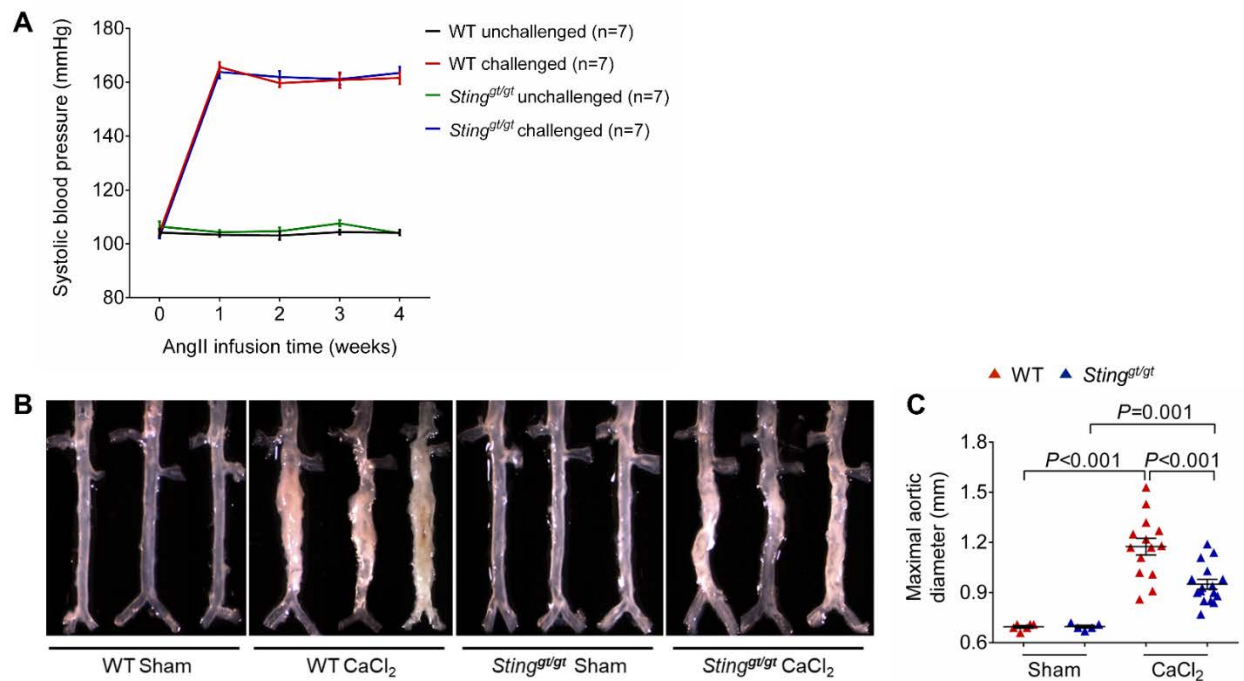
ssDNA and RNA (with low affinity), most of the signal is likely from dsDNA.<sup>17-19</sup> To detect cytosolic DNA in aortic tissues, we double-stained tissue sections for DNA (anti-dsDNA antibody) and a mitochondrial marker (anti-Tomm20 antibody). Antibodies used for immunofluorescence staining are listed in Supplemental Table 2. The slides were mounted and observed with a Leica SP5 confocal microscope (Leica Biosystems). The images were captured and analyzed by using LAS AF Lite software (Leica Biosystems).

### **Statistical Analyses**

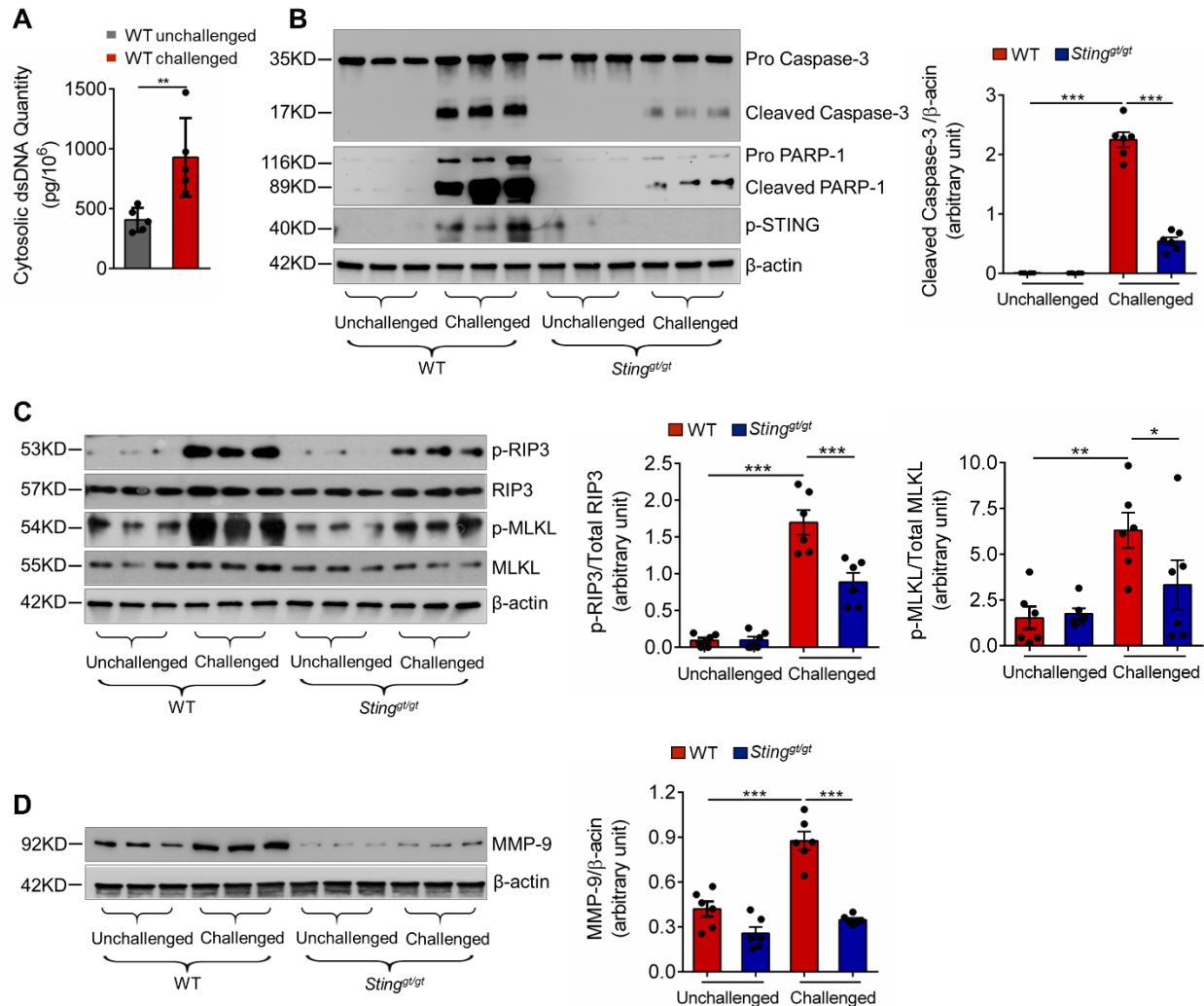
Normality of the data was examined by using the Kolmogorov-Smirnov test. We used an independent *t* test to make comparisons between two groups and a one-way analysis of variance (ANOVA) or the Kruskal-Wallis test, as appropriate, to make comparisons among multiple groups. One-way ANOVA with the Tukey post-hoc test for pairwise comparisons was used for equal variances. One-way ANOVA with Dunnett's T3 post-hoc test for pairwise comparisons was used for unequal variances. Two-way ANOVA was used to analyze the differences in two independent variables between groups. *P*-values were adjusted by using the Bonferroni method for pairwise comparisons, when indicated. Multi-way ANOVA was used to analyze the differences in several independent variables between groups, with the Holm-Šidák test used for pairwise comparisons. The incidence of AAD was analyzed by using the Fisher exact test. Kaplan-Meier survival curves were plotted to examine mouse survival rates, and the differences were analyzed by using the log-rank (Mantel-Cox) test. For all statistical analyses, 2-tailed probability values were used. A probability value of  $P < 0.05$  was considered significant.



**Supplemental Figure 1. Activation of the STING signaling pathway in human sporadic ascending thoracic aortic aneurysm and dissection (ATAAD) tissues.** **A**, Quantification of immunoblot data from Fig. 1A, showing STING pathway activation (ie, phosphorylated STING, TBK1, and IRF3). **B**, Representative immunostained images of ascending thoracic aortic dissection (ATAD) tissues showing CD68-positive cells in the media-adventitia boundary area, with high expression of STING and IRF3. For the quantified immunoblot data from Fig.1A, data were derived from patients with ascending thoracic aortic aneurysm (ATAA; n = 10), patients with acute ATAD (n = 10), and organ donors (control ascending aortic tissue, n = 8). One-way ANOVA with the Tukey post-hoc test was used for pairwise comparisons. Data are presented as the mean  $\pm$  standard error of the mean.

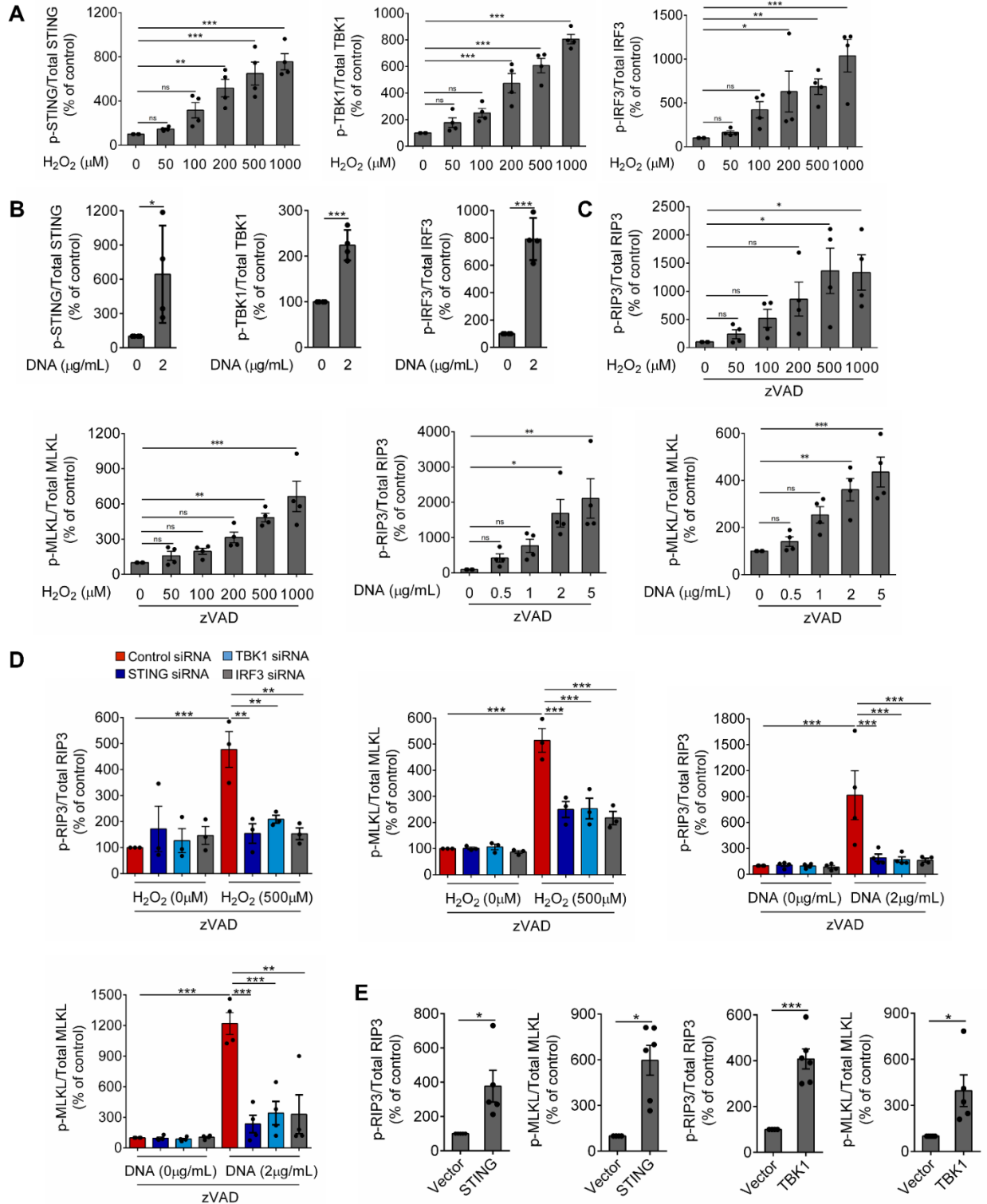


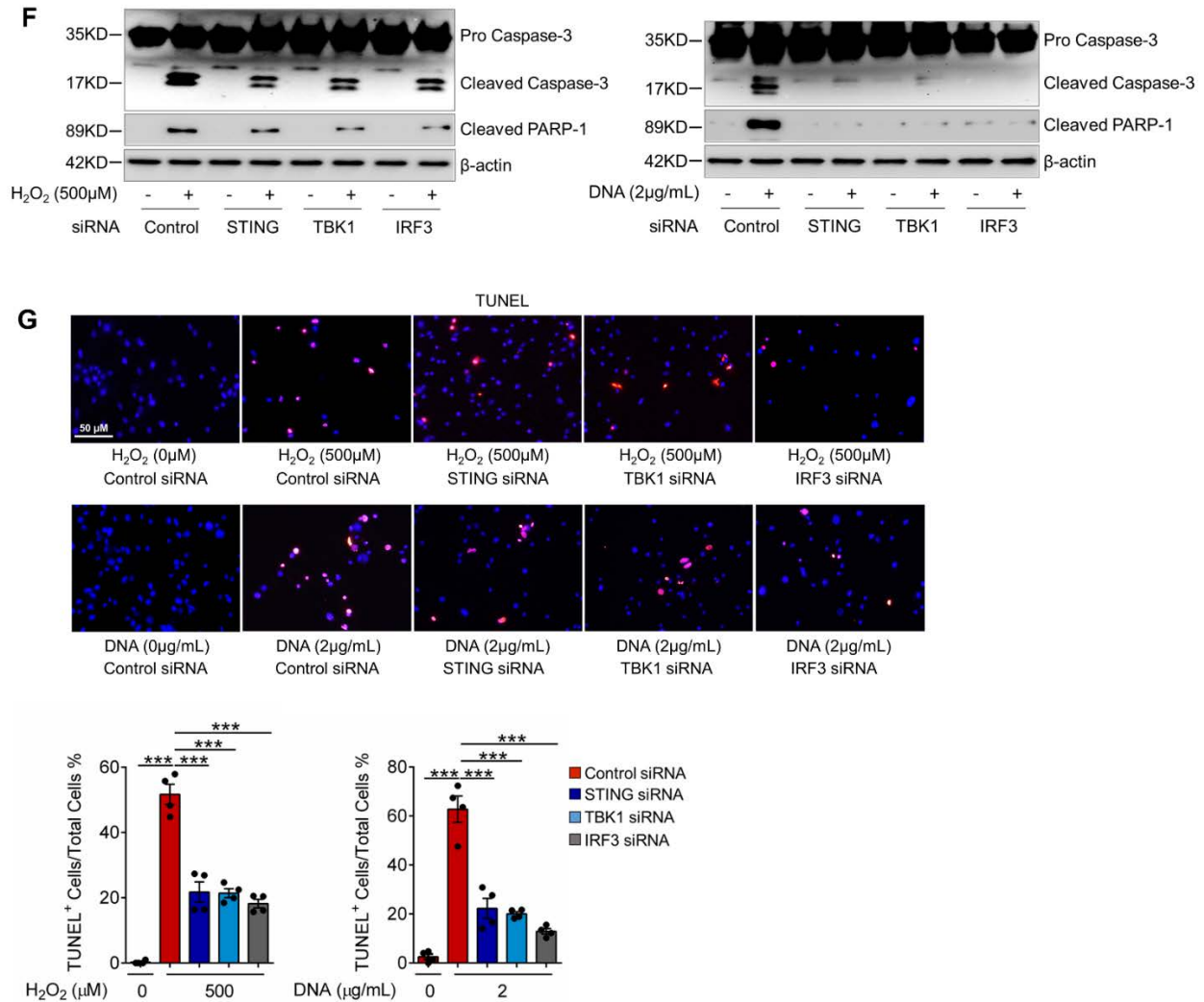
**Supplemental Figure 2. Reduced aortic enlargement in CaCl<sub>2</sub>-challenged *Sting*-deficient (*Sting*<sup>gt/gt</sup>) mice.** **A**, Wild-type (WT) mice and *Sting*<sup>gt/gt</sup> mice were unchallenged or challenged with a high-fat diet for 8 weeks and angiotensin II infusion (2000 ng/min/kg) during the last 4 weeks. Systolic blood pressure was similarly increased in WT and *Sting*<sup>gt/gt</sup> mice challenged with AngII (n=7 per group). **B**, WT mice and *Sting*<sup>gt/gt</sup> mice were unchallenged or challenged with CaCl<sub>2</sub>. Representative images of excised aortas showing less aortic enlargement in CaCl<sub>2</sub>-challenged *Sting*<sup>gt/gt</sup> mice than in CaCl<sub>2</sub>-challenged WT mice (n=5-16 per group). **C**, The maximal aortic diameters were smaller in CaCl<sub>2</sub>-challenged *Sting*<sup>gt/gt</sup> mice than in CaCl<sub>2</sub>-challenged WT mice (n=5-16 per group). Two-way ANOVA with the Bonferroni post-hoc test for pairwise comparisons was used for **(C)**. Data are presented as the mean ± standard error of the mean.



**Supplemental Figure 3. Prevention of challenge-induced smooth muscle cell (SMC) death and macrophage MMP-9 production in the suprarenal aorta of *Sting*-deficient (*Sting<sup>gt/gt</sup>*) mice.** Analyses were performed by using suprarenal aortas from wild-type (WT) mice and *Sting<sup>gt/gt</sup>* mice that were unchallenged or challenged with a high-fat diet for 8 weeks and angiotensin II infusion (2000 ng/min/kg) during the last 4 weeks. **A**, Bar graph showing that the quantity of cytosolic dsDNA in aortic cells of the suprarenal aorta was increased in challenged wild-type (WT) mice compared with unchallenged WT mice (n = 5 per group). **B**, Western blot

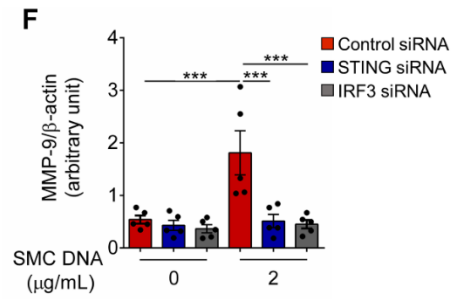
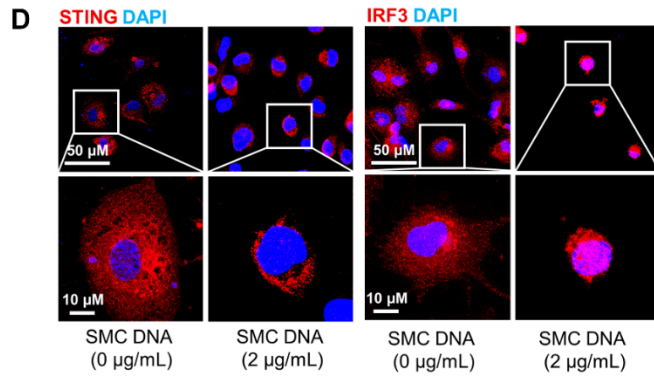
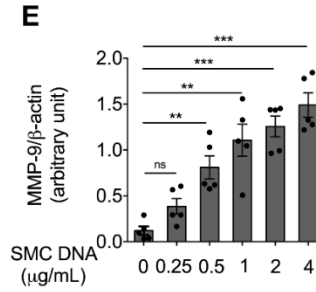
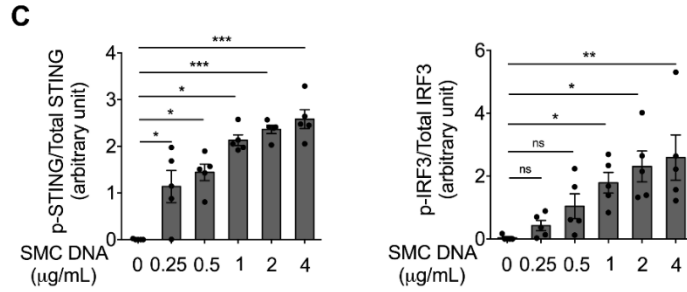
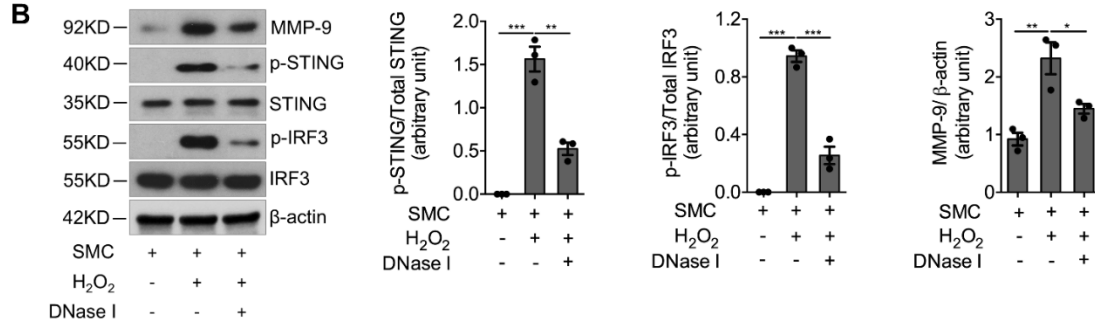
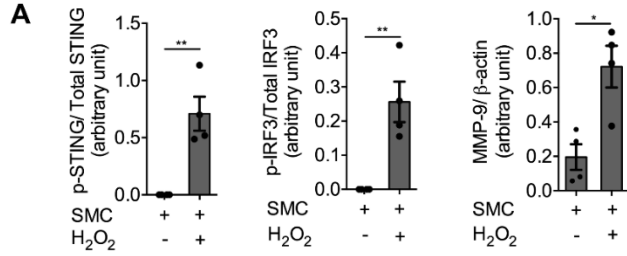
analysis and quantification data showing that the cleavage of caspase-3 and PARP-1 in the suprarenal aorta was reduced in challenged *Sting<sup>gt/gt</sup>* mice compared with challenged WT mice (n = 6 per group). Western blot analysis showing that aortic challenge in WT mice induced a marked increase in the level of phosphorylated STING in the suprarenal aorta. **C**, Western blot analysis and quantification data showing that the levels of p-RIP3 and p-MLKL in the suprarenal aorta were reduced in challenged *Sting<sup>gt/gt</sup>* mice compared with challenged WT mice (n = 6 per group). **D**, Western blot analysis and quantification showing that MMP-9 expression in the suprarenal aorta was reduced in challenged *Sting<sup>gt/gt</sup>* mice compared with challenged WT mice (n = 6 per group). An unpaired, two-tailed *t*-test was used in **(A)**. Two-way ANOVA with the Bonferroni post-hoc test was used for pairwise comparisons in **(B)** through **(D)**. \**P* < 0.05, \*\**P* < 0.01, \*\*\**P* < 0.001. Data are presented as the mean ± standard error of the mean.

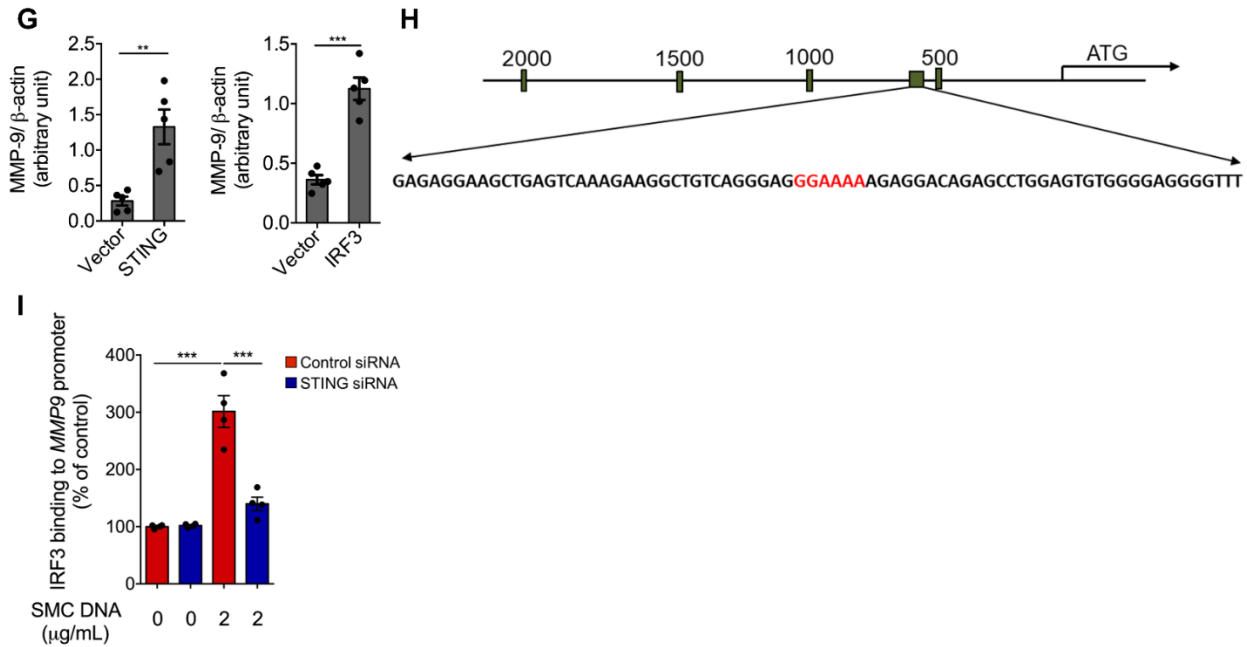




**Supplemental Figure 4. Critical role of the STING-TBK1-IRF3 pathway in aortic smooth muscle cell (SMC) injury.** **A**, Quantification of immunoblot data from Fig. 5C, showing increased phosphorylation of STING, TBK1, and IRF3 in SMCs treated with H<sub>2</sub>O<sub>2</sub> (n=4 biologic repeats). **B**, Quantification of immunoblot data from Fig. 5D, showing increased phosphorylation of STING, TBK1 and IRF3 in smooth muscle cells (SMCs) treated with exogenous SMC DNA (n=4 biologic repeats). **C**, Quantification of immunoblot data from Fig. 5G, showing that H<sub>2</sub>O<sub>2</sub> or exogenous SMC DNA induced the phosphorylation of RIP3 and MLKL in a dose-dependent manner in SMCs pretreated with zVAD (n=4 biologic repeats). **D**, Quantification of immunoblot

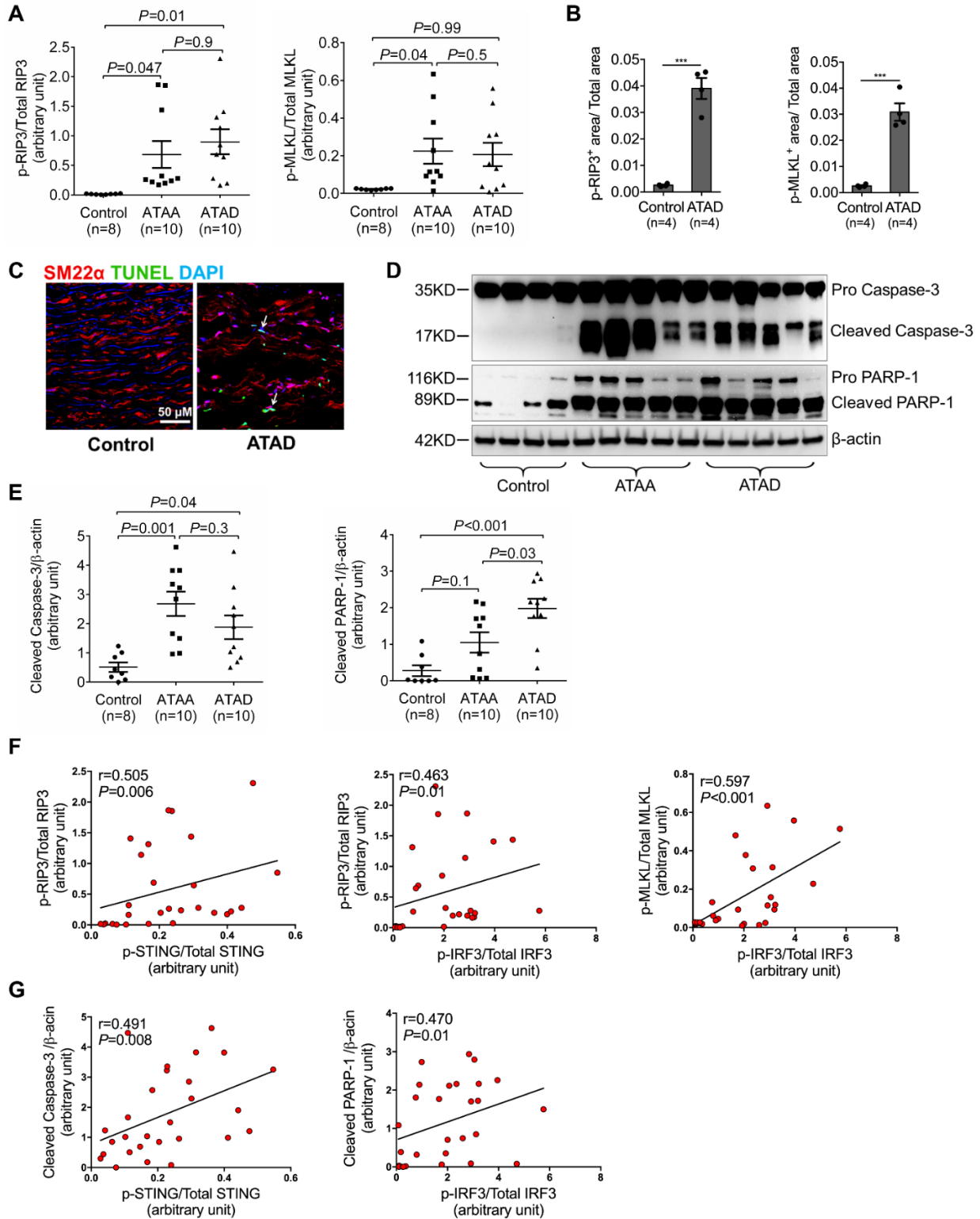
data from Fig. 5H, showing that silencing STING, TBK1, or IRF3 with siRNA prevented the H<sub>2</sub>O<sub>2</sub>-induced or exogenous SMC DNA-induced activation and phosphorylation of RIP3 and MLKL in SMCs pretreated with zVAD (n = 3 or 4 biologic repeats). **E**, Quantification of immunoblot data from Fig. 5I, showing that the overexpression of STING and TBK1 increased the activation and phosphorylation of RIP3 and MLKL in SMCs pretreated with zVAD (n = 5 or 6 biologic repeats). **F**, Western blot results showing that silencing STING, TBK1, or IRF3 with siRNA prevented the H<sub>2</sub>O<sub>2</sub>- or exogenous SMC DNA-induced cleavage of caspase-3 and PARP-1. **G**, Representative terminal deoxynucleotidyl transferase dUTP nick end labeling (TUNEL) staining shows that silencing STING, TBK1, or IRF3 with siRNA prevented SMC apoptosis induced by H<sub>2</sub>O<sub>2</sub> or exogenous SMC DNA (n=4 biologic repeats). One-way ANOVA with the Tukey post-hoc test was used for pairwise comparisons in **(A)**, **(C)**, and **(G)**. An unpaired, two-tailed *t*-test was used for **(B)** and **(E)**. Two-way ANOVA with the Bonferroni post-hoc test was used for pairwise comparisons in **(D)**. ns indicates not significant. \**P* < 0.05, \*\**P* < 0.01, \*\*\**P* < 0.001. Data are presented as the mean ± standard error of the mean.

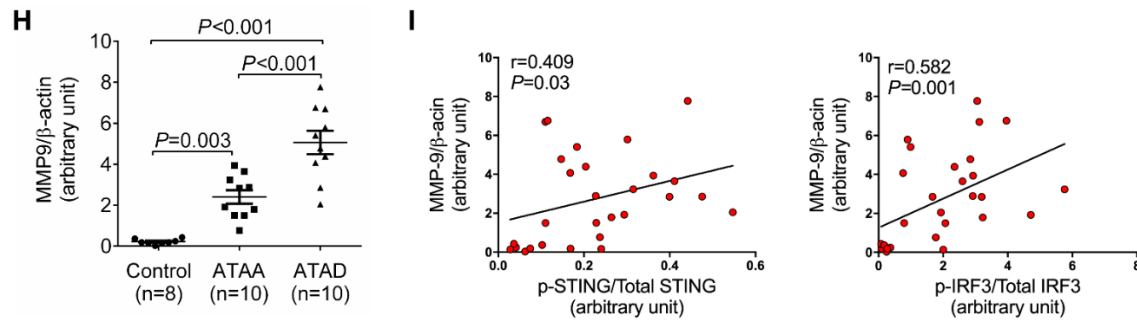




**Supplemental Figure 5. MMP-9 production in macrophages induced by DNA derived from H<sub>2</sub>O<sub>2</sub>-treated aortic smooth muscle cells (SMCs) through the activation of STING pathway.** **A**, Quantification of immunoblot data from Fig. 6C, showing STING pathway activation (phosphorylated STING and IRF3) and MMP-9 production in macrophages co-cultured with H<sub>2</sub>O<sub>2</sub>-treated smooth muscle cells (SMCs) (n = 4 biologic repeats). **B**, Western blot analysis and quantification data showing that STING pathway activation and MMP-9 production in macrophages co-cultured with H<sub>2</sub>O<sub>2</sub>-treated SMCs were reduced with DNase I (1 μg/mL) treatment (n = 3 biologic repeats). **C**, Quantification of immunoblot data from Fig. 6D, showing that the activation of the STING pathway was increased in a dose-dependent manner in macrophages treated with SMC DNA, manifested as increased phosphorylation of STING and IRF3 (n = 5 biologic repeats). **D**, SMC derived DNA stimulated STING and IRF3 perinuclear and nuclear translocation (n = 5 biologic repeats). Insets show a higher-magnification view. **E**, Quantification of immunoblot data from Fig. 6E, showing that the expression of MMP-9 was significantly increased in a dose-dependent manner after treatment with SMC DNA (n = 5

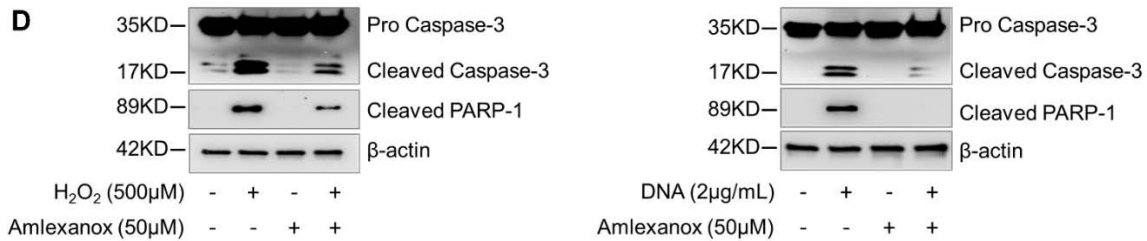
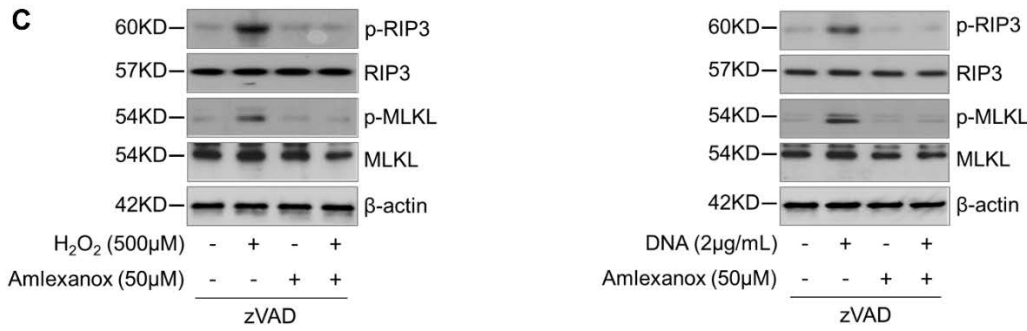
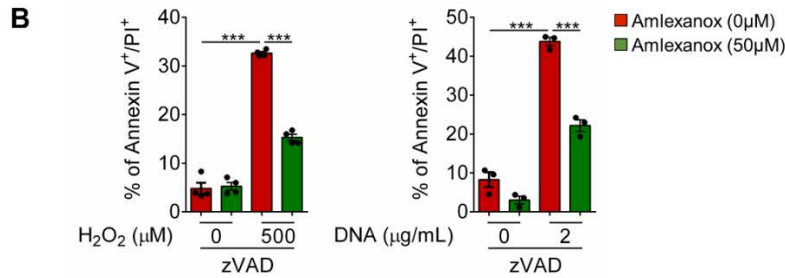
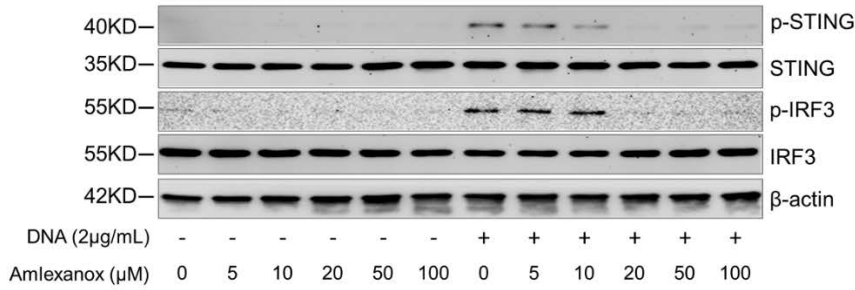
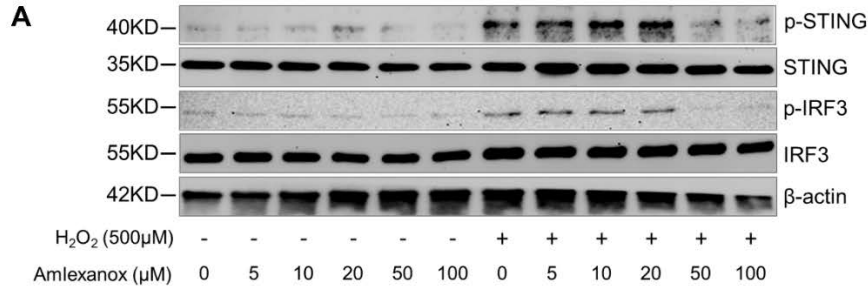
biologic repeats). **F**, Quantification of immunoblot data from Fig. 6H, showing that the increase in MMP-9 expression induced by SMC DNA was reduced in macrophages transfected with STING siRNA or IRF3 siRNA (n = 5 biologic repeats). **G**, Quantification of immunoblot data from Fig. 6H, showing that the level of MMP-9 was increased in macrophages transfected with STING or IRF3 plasmid (n = 5 biologic repeats). **H**, A putative IRF3 binding site upstream of the 5'-untranslated region of *MMP9* is shown in red. **I**, Quantification of chromatin immunoprecipitation assay data showing that the binding of IRF3 to the *MMP9* promoter was increased in macrophages treated with SMC DNA and that this binding was abolished by silencing STING expression with STING siRNA (n = 4 biologic repeats). An unpaired, two-tailed *t*-test was used in **(A)** and **(G)**. One-way ANOVA with the Tukey post-hoc test for pairwise comparisons was used for **(B)**, **(C)**, and **(E)**. Two-way ANOVA with the Bonferroni post-hoc test for pairwise comparisons was used for **(F)** and **(I)**. ns indicates not significant. \**P* < 0.05, \*\**P* < 0.01, \*\*\**P* < 0.001. Data are presented as the mean ± standard error of the mean.

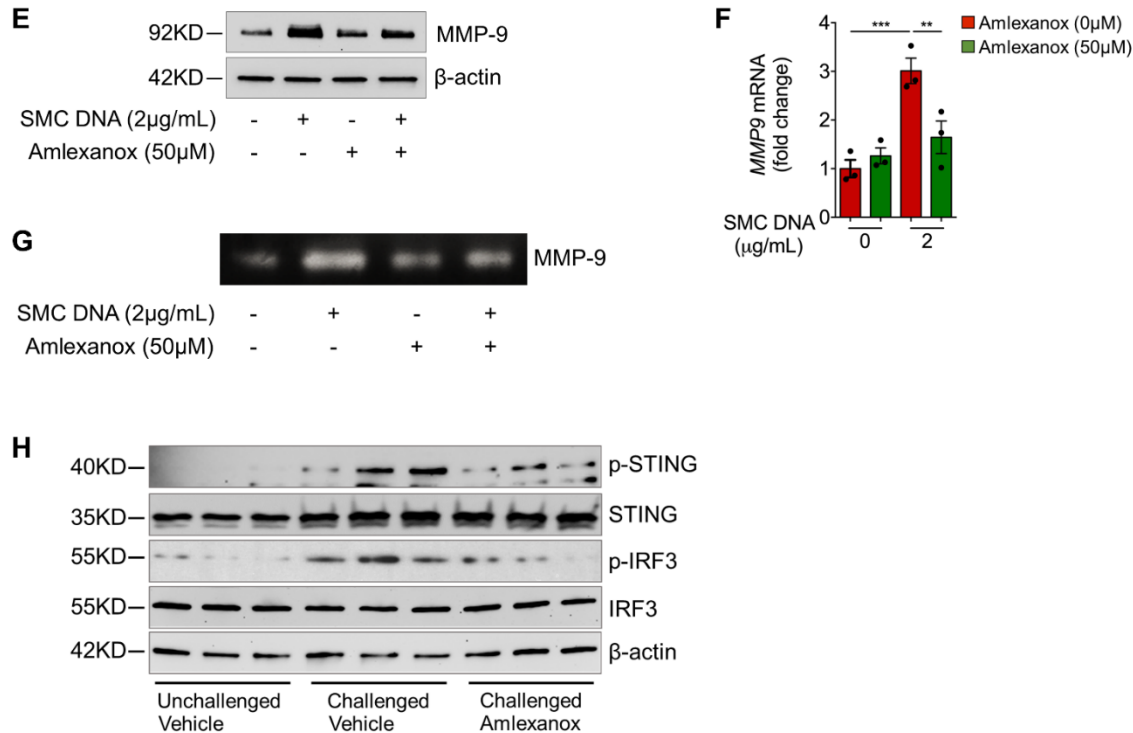




**Supplemental Figure 6. Association of STING activation with smooth muscle cell (SMC) injury and macrophage MMP-9 production in human sporadic ascending thoracic aortic aneurysm and dissection (ATAAD) tissues.** **A**, Quantification of immunoblot data from Fig. 7B, showing activation of the necroptosis pathway (ie, phosphorylated RIP3 and MLKL). **B**, Quantification of immunofluorescence staining from Fig. 7C showing increased p-RIP3 and p-MLKL expression in aortas from patients with ascending thoracic aortic dissection (ATAD) (n=4). **C**, Representative terminal deoxynucleotidyl transferase dUTP nick end labeling (TUNEL)-stained images of ascending aortic sections showing an increased number of apoptotic cells in the aortic wall of patients with ATAD. **D**, Western blot analysis showing increased cleavage of caspase-3 and PARP-1 in the aortic wall of patients with ascending thoracic aortic aneurysm and dissection (ATAAD). **E**, Quantification of immunoblot data from Supplemental Figure 6D, showing activation of the apoptosis pathway (ie, cleaved caspase-3 and PARP-1). Correlation analysis showing that the activation of necroptosis pathway **F**, and the apoptosis pathway **G**, were correlated with STING-TBK1-IRF3 pathway activation. **H**, Quantification of immunoblot data from Fig. 7E, showing increased MMP-9 expression in aortic tissues from patients with ascending thoracic aortic aneurysm (ATAA) and patients with acute ATAD. **I**, Correlation analysis showing that MMP-9 production was correlated with STING pathway activation. For the quantified immunoblot data from Fig.6, data were derived from patients with ATAA (n = 10), patients with acute ATAD (n = 10), and organ donors (control

ascending aortic tissue,  $n = 8$ ). One-way ANOVA with the Dunnett's T3 post-hoc test for pairwise comparisons was used in **(A)**. One-way ANOVA with the Tukey post-hoc test for pairwise comparisons was used in **(A)**, **(E)**, and **(H)**.  $***P < 0.001$ . Spearman rank correlation analysis was used for **(F)**, **(G)**, and **(I)**. Data are presented as the mean  $\pm$  standard error of the mean.





**Supplemental Figure 7. Prevention of smooth muscle cell (SMC) injury and macrophage MMP-9 production by amlexanox.** **A**, In cultured SMCs treated with H<sub>2</sub>O<sub>2</sub> or exogenous SMC DNA, dose-response relationship of amlexanox determined by phosphorylation of STING and IRF3. **B**, Flow cytometry analysis showing that amlexanox partially decreased the necroptotic cell death induced by H<sub>2</sub>O<sub>2</sub> or exogenous SMC DNA (n = 3 or 4 biologic repeats). **C**, Western blot analysis showing that amlexanox partially the H<sub>2</sub>O<sub>2</sub>- or exogenous SMC DNA–induced activation and phosphorylation of RIP3 and MLKL in SMCs pretreated with zVAD. **D**, Western blot analysis showing that amlexanox partially prevented the H<sub>2</sub>O<sub>2</sub>- or exogenous SMC DNA–induced cleavage of caspase-3 and PARP-1. Amlexanox partially decreased the MMP-9 production in THP-1 differentiated macrophages treated with SMC-derived DNA in protein level (**E**), mRNA level (**F**) and MMP-9 activity (**G**). **H**, Western blot analysis showing the activation of STING pathway in challenged mice compared with unchallenged mice. With the treatment of Amlexanox, the phosphorylation of STING and IRF3 decreased significantly (n=3 per group).

Two-way ANOVA with the Bonferroni post-hoc test was used for pairwise comparisons in **(B)** and **(F)**. \*\* $P < 0.01$ , \*\*\* $P < 0.001$ . Data are presented as the mean  $\pm$  standard error of the mean.

**Supplemental Table 1. Patient Characteristics**

<b>Characteristics</b>	<b>Control (n=8)</b>	<b>ATAA (n=10)</b>	<b>ATAD (n=10)</b>
Age (y)	69.9 ± 7.1	62.8 ± 8.6	61.2 ± 8.7
Men	4 (50%)	6 (60%)	6 (60%)
Hypertension	8 (100%)	8 (80%)	10 (100%)
COPD	0	0	2 (20%)
Diabetes mellitus	1 (13%)	1 (10%)	2 (20%)
History of smoking	2 (25%)	3 (30%)	3 (30%)
Use of antilipid medication	3 (38%)	5 (50%)	0
Use of COX inhibitor	4 (50%)	5 (50%)	3 (30%)
Aortic diameter (cm)	NA	5.3 ± 0.9	5.2 ± 1

Data are expressed as a number (percent) or as the mean ± standard deviation. ATAA indicates ascending thoracic aortic tissue from patients with ascending thoracic aortic aneurysm; ATAD, ascending thoracic aortic tissue from patients with acute ascending thoracic aortic dissection; COPD, chronic obstructive pulmonary disease; COX, cyclooxygenase; NA, not available.

**Supplemental Table 2. Antibodies Used for Western Blot and Immunostaining Experiments**

<b>Antibody</b>	<b>Vendor name</b>	<b>Catalog number</b>	<b>Dilution</b>
Western blot analysis			
Primary antibody			
Anti-STING (D2P2F)	Cell Signaling	13647	1:1000
Anti-phospho-STING (Ser366)	Cell Signaling	85735	1:500
Anti-phospho-STING (Ser365)	Cell Signaling	72971	1:500
Anti-TBK1	Abcam	ab-40676	1:1000
Anti-phospho-TBK1 (Ser172)	Abcam	ab-109272	1:1000
Anti-IRF-3	Cell Signaling	4302	1:1000
Anti-phospho-IRF3 (Ser396)	Cell Signaling	4947	1:500
Anti-MMP-9	Cell Signaling	13667	1:1000
Anti-MMP-9	Santa Cruz	sc-6840	1:500
Anti-RIP3	Santa Cruz	sc-374639	1:500
Anti-phospho-RIP3 (Ser227)	Abcam	ab-209384	1:500
Anti-phospho-RIP3 (Ser232)	Abcam	ab-195117	1:1000
Anti-MLKL	Millipore	17-10400	1:1000
Anti-MLKL	Thermo Fisher Scientific	PA5-43960	1:1000

Anti-phospho-MLKL (Ser358)	Millipore	17-10400	1:500
Anti-phospho-MLKL (Ser345)	Abcam	ab-196436	1:500
Anti- Caspase-3	Cell Signaling	9662	1:800
Anti-Cleaved PARP	Abcam	136812	1:500
Anti-Cleaved PARP	Cell Signaling	5625	1:500
Anti- $\beta$ -Actin	Santa Cruz	sc-47778	1:5000
Secondary antibody			
Anti-rabbit IgG, HRP-linked antibody	Cell Signaling	7074	1:5000
Anti-mouse IgG, HRP-linked antibody	Cell Signaling	7076	1:5000
Immunostaining			
Primary antibody			
Anti-dsDNA	Abcam	ab-27156	1:200
Anti-TOMM20	Abcam	ab-78547	1:200
Anti-Lamp1	Cell Signaling	9091	1:200
Anti- SM22- $\alpha$	Abcam	ab-10135	1:200
Anti-CD68	Abcam	ab-955	1:100
Anti-STING	Thermo Fisher Scientific	PA5-20782	1:200
Anti-STING	Novus Biologicals	723505	1:300

Anti-TBK1	Abcam	ab-40676	1:200
Anti-IRF3	Abcam	ab-68481	1:200
Anti-IRF3	Santa Cruz	sc-376455	1:200
Anti-MMP-9	Santa Cruz	sc-6840	1:100
Anti-phospho-RIP3(Ser227)	Cell Signaling	93654	1:200
Anti- phospho-RIP3 (Thr231/Ser232)	Cell Signaling	91702	1:200
Anti-phospho-MLKL(Ser358)	Abcam	ab-187091	1:200
Anti-phospho-MLKL(Thr357)	Novus Biologicals	954724	1:300
Anti-phospho-MLKL (Ser345)	Abcam	ab-196436	1:200
Secondary antibody			
Alexa Fluor™ 568 donkey anti-goat IgG (H+L)	Invitrogen	A11057	1:200
Alexa Fluor™ 568 donkey anti-mouse IgG (H+L)	Invitrogen	A10037	1:200
Alexa Fluor™ 488 donkey anti-rabbit IgG (H+L)	Invitrogen	A32790	1:200
Alexa Fluor™ 488 donkey anti-mouse IgG (H+L)	Invitrogen	A32766	1:200
Alexa Fluor™ 488 donkey anti-goat IgG (H+L)	Invitrogen	A11055	1:200
Alexa Fluor™ 680 donkey anti-goat IgG (H+L)	Invitrogen	A21084	1:200
Alexa Fluor™ 647 donkey anti-mouse IgG (H+L)	Invitrogen	A31571	1:200
Alexa Fluor™ 680 donkey anti-rabbit IgG (H+L)	Invitrogen	A10043	1:200

---

Alexa Fluor™ 568 donkey anti-rabbit IgG (H+L)	Invitrogen	A10042	1:200
---	------------	--------	-------

---

HRP, horseradish peroxidase.

## References

1. Ren P, Hughes M, Krishnamoorthy S, Zou S, Zhang L, Wu D, Zhang C, Curci JA, Coselli JS, Milewicz DM, LeMaire SA, Shen YH. Critical role of ADAMTS-4 in the development of sporadic aortic aneurysm and dissection in mice. *Sci Rep.* 2017;7:12351. doi: 10.1038/s41598-017-12248-z.
2. Wu D, Ren P, Zheng Y, Zhang L, Xu G, Xie W, Lloyd EE, Zhang S, Zhang Q, Curci JA, Coselli JS, Milewicz DM, Shen YH, LeMaire SA. NLRP3 (nucleotide oligomerization domain-like receptor family, pyrin domain containing 3)-caspase-1 inflammasome degrades contractile proteins: implications for aortic biomechanical dysfunction and aneurysm and dissection Formation. *Arterioscler Thromb Vasc Biol.* 2017;37:694-706. doi: 10.1161/ATVBAHA.116.307648.
3. Chiou AC, Chiu B, Pearce WH. Murine aortic aneurysm produced by periarterial application of calcium chloride. *J Surg Res.* 2001;99:371-376. doi: 10.1006/jsre.2001.6207.
4. Ghaghada KB, Badea CT, Karumbaiah L, Fettig N, Bellamkonda RV, Johnson GA, Annapragada A. Evaluation of tumor microenvironment in an animal model using a nanoparticle contrast agent in computed tomography imaging. *Acad Radiol.* 2011;18:20-30. doi: 10.1016/j.acra.2010.09.003.
5. Starosolski Z, Villamizar CA, Rendon D, Paldino MJ, Milewicz DM, Ghaghada KB, Annapragada AV. Ultra high-resolution in vivo computed tomography imaging of mouse cerebrovasculature using a long circulating blood pool contrast agent. *Sci Rep.* 2015;5:10178. doi: 10.1038/srep10178.
6. Annapragada AV, Hoffman E, Divekar A, Karathanasis E, Ghaghada KB. High-resolution CT vascular imaging using blood pool contrast agents. *Methodist DeBakey Cardiovasc J.* 2012;8:18-22.

7. Daugherty A, Manning MW, Cassis LA. Angiotensin II promotes atherosclerotic lesions and aneurysms in apolipoprotein E-deficient mice. *J Clin Invest.* 2000;105:1605-1612. doi: 10.1172/JCI7818.
8. LeMaire SA, Zhang L, Luo W, Ren P, Azares AR, Wang Y, Zhang C, Coselli JS, Shen YH. Effect of ciprofloxacin on susceptibility to aortic dissection and rupture in mice. *JAMA Surg.* 2018;153:e181804. doi: 10.1001/jamasurg.2018.1804.
9. Trapnell C, Williams BA, Pertea G, Mortazavi A, Kwan G, van Baren MJ, Salzberg SL, Wold BJ, Pachter L. Transcript assembly and quantification by RNA-Seq reveals unannotated transcripts and isoform switching during cell differentiation. *Nat Biotechnol.* 2010;28:511-515. doi: 10.1038/nbt.1621.
10. Robinson MD, McCarthy DJ, Smyth GK. edgeR: a Bioconductor package for differential expression analysis of digital gene expression data. *Bioinformatics.* 2010;26:139-140. doi: 10.1093/bioinformatics/btp616.
11. Yu G, Wang LG, Han Y, He QY. clusterProfiler: an R package for comparing biological themes among gene clusters. *OMICS.* 2012;16:284-287. doi: 10.1089/omi.2011.0118.
12. Butler A, Hoffman P, Smibert P, Papalexi E, Satija R. Integrating single-cell transcriptomic data across different conditions, technologies, and species. *Nat Biotechnol.* 2018;36:411-420. doi: 10.1038/nbt.4096.
13. Jonsson KL, Laustsen A, Krapp C, Skipper KA, Thavachelvam K, Hotter D, Egedal JH, Kjolby M, Mohammadi P, Prabakaran T, Sorensen LK, Sun C, Jensen SB, Holm CK, Lebbink RJ, Johannsen M, Nyegaard M, Mikkelsen JG, Kirchhoff F, Paludan SR, Jakobsen MR. IFI16 is required for DNA sensing in human macrophages by promoting production and function of cGAMP. *Nat Commun.* 2017;8:14391. doi: 10.1038/ncomms14391.
14. Mao Y, Luo W, Zhang L, Wu W, Yuan L, Xu H, Song J, Fujiwara K, Abe JI, LeMaire SA, Wang XL, Shen YH. STING-IRF3 triggers endothelial inflammation in response to free

- fatty acid-induced mitochondrial damage in diet-induced obesity. *Arterioscler Thromb Vasc Biol.* 2017;37:920-929. doi: 10.1161/ATVBAHA.117.309017.
15. Shen YH, Zhang L, Ren P, Nguyen MT, Zou S, Wu D, Wang XL, Coselli JS, LeMaire SA. AKT2 confers protection against aortic aneurysms and dissections. *Circ Res.* 2013;112:618-632.
  16. Yuan L, Mao Y, Luo W, Wu W, Xu H, Wang XL, Shen YH. Palmitic acid dysregulates the Hippo-YAP pathway and inhibits angiogenesis by inducing mitochondrial damage and activating the cytosolic DNA sensor cGAS-STING-IRF3 signaling mechanism. *J Biol Chem.* 2017;292:15002-15015. doi: 10.1074/jbc.M117.804005.
  17. Aparicio R, Rana A, Walker DW. Upregulation of the autophagy adaptor p62/SQSTM1 prolongs health and lifespan in middle-aged drosophila. *Cell Reports.* 2019;28:1029-1040.e1025. doi: <https://doi.org/10.1016/j.celrep.2019.06.070>.
  18. Rana A, Oliveira MP, Khamoui AV, Aparicio R, Rera M, Rossiter HB, Walker DW. Promoting Drp1-mediated mitochondrial fission in midlife prolongs healthy lifespan of *Drosophila melanogaster*. *Nat Commun.* 2017;8:448. doi: 10.1038/s41467-017-00525-4.
  19. Vanpouille-Box C, Alard A, Aryankalayil MJ, Sarfraz Y, Diamond JM, Schneider RJ, Inghirami G, Coleman CN, Formenti SC, Demaria S. DNA exonuclease Trex1 regulates radiotherapy-induced tumour immunogenicity. *Nat Commun.* 2017;8:15618. doi: 10.1038/ncomms15618.